








Au-induced reconstructions of the Si(111) surface with ordered and disordered domain wallsL. V. Bondarenko ^{1,*}, A. N. Mihalyuk ^{1,2}, A. Y. Tupchaya ¹, Y. E. Vekovshinin ^{1,2}, D. V. Gruznev ¹,
A. V. Zotov ¹ and A. A. Saranin ¹¹*Institute of Automation and Control Processes FEB RAS, 690041 Vladivostok, Russia*²*School of Natural Sciences, Far Eastern Federal University, 690950 Vladivostok, Russia*

(Received 25 November 2019; accepted 17 January 2020; published 4 February 2020)

Scanning tunneling microscopy (STM) and angle-resolved photoemission spectroscopy (ARPES) observations combined with the density functional theory (DFT) calculations were used to elucidate atomic arrangement of Au/Si(111) reconstructions forming at Au coverage around one monolayer. They include the Si(111)6 × 6-Au with ordered domain walls, the Si(111)α − √3 × √3-Au and the Si(111)β − √3 × √3-Au surfaces with disordered domain walls of various density, and the Si(111)2√21 × 2√21-Au surface which structure is relevant to those of other reconstructions, albeit cannot be ascribed solely to the domain walls. Using detailed comparison of the STM and ARPES data with the results of DFT calculations, we explicitly proved the atomic model of Si(111)6 × 6-Au surface proposed by Grozea *et al.* [*Surf. Sci.* **418**, 32 (1998)]. This model provided us a hint for constructing an atomic model of domain walls which demonstrates a proper coincidence between experimental and simulated STM images. The model contains five Au atoms per 2 × √3 unit cell, i.e., 1.25 monolayers of Au. For the α − √3 × √3-Au and β − √3 × √3-Au surfaces, this finding allows an overall description of their atomic arrangement and, hence, accurate determination of their Au coverages. Knowledge on the atomic arrangement of the Si(111)6 × 6-Au surface and domain walls also allowed us to construct an atomic model of the Si(111)2√21 × 2√21-Au surface. The obtained data were unified in the refined formation phase diagram for the Au/Si(111) system.

DOI: [10.1103/PhysRevB.101.075405](https://doi.org/10.1103/PhysRevB.101.075405)**I. INTRODUCTION**

Gold-induced reconstructions on the Si(111) surface have been extensively studied since 1964, when the Si(111)6 × 6-Au reconstruction was first observed with low-energy electron diffraction [1]. In the subsequent years, a set of other reconstructions were found, including 5 × 2-Au [2], √3 × √3-Au [2] (subdivided later in the two phases [3], namely α − √3 × √3-Au and β − √3 × √3-Au), and 2√21 × 2√21-Au [4,5]. Such abundance of atomic structures and, hence, properties associated with them have stimulated active researches of monolayer and submonolayer Au/Si(111) systems and substantial attention to them remains nowadays. The most vivid example is the Si(111)5 × 2-Au surface which presents itself as a self-organized one-dimensional metal chain system [6–10] and has served as a rich source of one-dimensional (1D) phenomena such as atomic-scale Schottky barriers [11,12], 1D domain-wall hoppings [13], and confined doping on a metallic chain [14,15]. Another example is Si(111)√3 × √3-Au surface which being modified by adsorption of In, Tl, or Cs has been found to demonstrate a giant Rashba-type spin splitting of metallic surface-state bands [16]. Moreover, recent DFT calculations have predicted that Si(111)√3 × √3-Au surface covered with heavy metals (e.g., Bi, Tl, In, Pb, or Sb) shows promise for possessing properties two-dimensional (2D) topological insulators (known also as quantum spin Hall insulators) [17–19].

Worth noting that besides the 5 × 2-Au reconstruction which forms at nominal Au coverage of 0.7 ML [20] (monolayer, 1 ML equals to 7.8 × 10¹⁴ cm^{−2}), all the other reconstructions are observed at Au coverages of about 1.0 ML and beyond and formation of a particular phase depends on the growth procedure. In particular, α − √3 × √3-Au and β − √3 × √3-Au phases are formed upon depositing Au (with Au coverage being greater for the β − √3 phase than for the α − √3 phase), followed by rapid cooling (quenching) to room temperatures (RT). In both cases, the surface consists of √3 × √3 domains separated by disordered network of the domain walls (DWs). Atomic structure within √3 × √3 domains is described by the conjugate honeycomb-chained-trimer (CHCT) model [21]. In the α − √3 phase, the √3 × √3 domains are relatively large, while in the β − √3 phase the areas occupied by domains and DWs are almost the same. The 6 × 6 and 2√21 × 2√21 phases form upon slow cooling of β − √3 phase [22–24] and are thought to be domain-wall crystals due to ordering of the DWs. Thus, one can see that DW is a principal element of all these phases and elucidating atomic arrangement of DWs is a principal step on a way to accurate description of the Au/Si(111) reconstructions. Correct atomic model of the 6 × 6 phase could provide us a hint for building a correct atomic model of the DWs.

In the present work we show that our advanced angle-resolved photoemission spectroscopy (ARPES) and scanning tunneling microscopy (STM) data for Si(111)6 × 6-Au surface can be reasonably reproduced by density functional theory (DFT) calculations conducted on the basis of the 6 × 6 atomic model proposed by Grozea *et al.* [25]. In

*bondarenko@dvo.ru

particular, it becomes even possible to clarify the origin of the inhomogeneity of the Si(111) 6×6 -Au surface, as arising from occurrence of three specific positions partially occupied by Au atoms. Statistical analysis yields that the 6×6 unit cell contains in average 43.58 Au atoms, i.e., 1.21 ML of Au. We show then that atomic model of DWs extracted from the model of the Si(111) 6×6 -Au surface provides a fairly good coincidence of STM data with DFT simulations, in contrast with the previous model proposed by Falta *et al.* [26]. Novel atomic model of DW contains 5 Au atoms per $2 \times \sqrt{3}$ unit cell or 1.25 ML of Au. For the $\alpha - \sqrt{3}$ and $\beta - \sqrt{3}$ surfaces these findings allow overall description of their atomic structure and, hence, accurate determination of Au coverage. The gained knowledge also allowed us to construct a novel atomic model of the Si(111) $2\sqrt{21} \times 2\sqrt{21}$ -Au surface and to build the refined formation phase diagram for the Au/Si(111) system.

II. EXPERIMENTAL AND CALCULATION DETAILS

Experiments were performed in the ultrahigh-vacuum Omicron MULTIPROBE system with a base pressure better than 2.0×10^{-10} Torr equipped with STM, LEED, and ARPES facilities. Atomically clean Si(111) 7×7 surfaces were prepared *in situ* by flashing to 1280 °C after the samples were first outgassed at 600 °C for several hours. Au-induced reconstructions on the Si(111) surface were formed by depositing Au from a tungsten filament onto the Si(111) 7×7 surface with subsequent annealing at 600 °C following by quenching (few minutes) or slow (~ 10 °C/min) cooling to room temperature (RT). Au deposition rate was calibrated using STM observations of the formation of Si(111) 5×2 -Au surface with nominal Au coverage of 0.7 ML [20]. STM images were acquired using Omicron variable-temperature STM-XA operating in a constant-current mode. Mechanically cut PtIr tips were used as STM probes after annealing in vacuum. ARPES measurements were conducted using a VG Scienta R3000 electron analyzer and high-flux He discharge lamp ($h\nu = 21.2$ eV) with a toroidal-grating monochromator as a light source.

Density functional theory calculations were performed by using the Vienna *ab initio* simulation package (VASP) [27,28], with core electrons represented by projector augmented wave (PAW) potentials [29,30]. The Si(111) 6×6 -Au and the Si(111) $2\sqrt{21} \times 2\sqrt{21}$ -Au surfaces cell geometries was simulated by a repeating slab of four bilayers and a vacuum region of ~ 15 Å. Si atoms in the bottom bilayer were fixed at their bulk positions, top three bilayers were allowed to fully relax, and dangling bonds on the bottom surface were saturated by hydrogen atoms. The kinetic cutoff energy was 250 eV. A $2 \times 2 \times 1$ and a $1 \times 1 \times 1$ Γ -centered k -point meshes were used to sample the surface Brillouin zones of 6×6 and $2\sqrt{21} \times 2\sqrt{21}$ unit cells respectively. The geometry optimization was performed until the residual force became smaller than 10 meV/Å. For surface band structure calculations we used slab model and applied the DFT-1/2 self-energy correction method [31,32] which only requires the addition of a self-energy correction potential, calculated from a half-ionized free atom, to the standard DFT potential (PAW-LDA in our case).

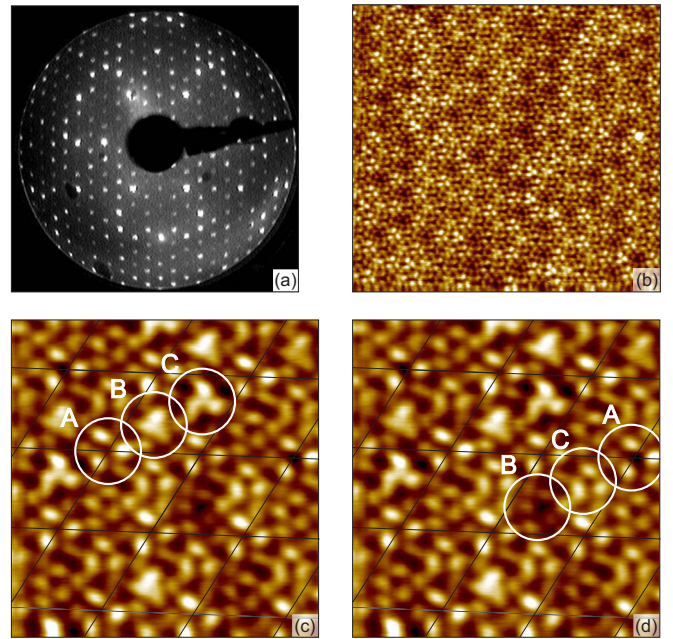


FIG. 1. Si(111) 6×6 -Au surface: (a) LEED pattern ($E_p = 62$ eV); (b) 50×50 nm² STM image ($V_s = -1.0$ V, $I = 50$ pA); (c) and (d) 8×8 nm² STM image ($V_s = -0.5$ V, $I = 50$ pA) with outlined (c) occupied and (d) unoccupied A, B, C positions.

III. RESULTS AND DISCUSSION

A. Si(111) 6×6 -Au: Atomic structure

Figure 1 illustrates typical LEED and STM appearance of Si(111) 6×6 -Au surface. Though displaying a bright and sharp LEED pattern [Fig. 1(a)], the 6×6 -Au surface looks quite inhomogeneous in the STM images [Fig. 1(b)]. This inhomogeneity shows up as randomly scattered bright and dim features and was already described in a detail by Higashiyama *et al.* [33]. They showed that each 6×6 unit cell has three different sites labelled as A, B, and C in Figs. 1(c) and 1(d), which can be occupied by an Au atom or not, consequently looks as bright or dim. Jałochowski [34] and Patterson [35] have tied these bright and dim features to specific sites in the atomic model of the Si(111) 6×6 proposed by Grozea *et al.* [25]. The basic model with only small atomic displacements upon relaxation found a confirmation in the recent x-ray diffraction [36] and DFT [35] studies. Such a relaxed model is depicted in Figs. 2(a) and 2(b) with specific Au atomic positions outlined by red circles. The model has a C_3 symmetry and, hence, two mirror domains [Figs. 2(a) and 2(b)]. Occurrence of mirror domains was proved in STM observations: in Fig. 2(c) both domains are present in a single STM image. The 6×6 atomic model can be visualized as an ordered stacking of the $\sqrt{3} \times \sqrt{3}$ CHCT “nanodomains,” each built of three Au trimers [outlined by red triangles in Figs. 2(a) and 2(b)] arranged into the local CHCT structure. Such nanodomains have minor differences in atomic structure resulting in different STM appearance as one can see in Figs. 1 and 2. Specific Au sites with partial occupancy are located in the centers of nanodomains and their occupancy determines whether they look bright or dim in the STM image. This picture can be intuitively suggested from available literature

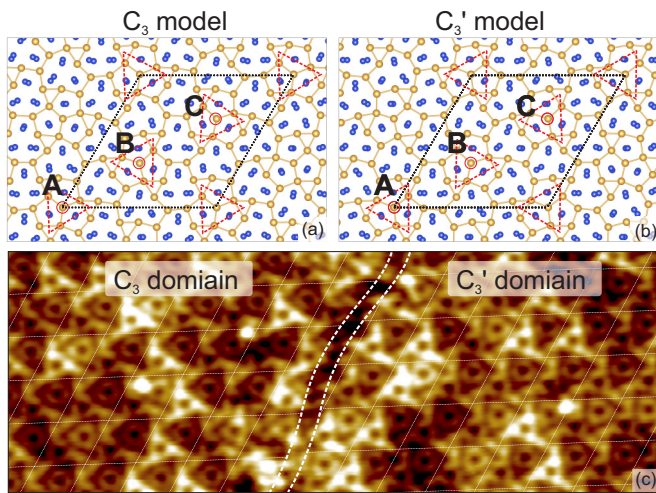


FIG. 2. (a) and (b) Two mirror domains of relaxed atomic model for Si(111)6 × 6-Au surface constructed on the basis of Grozea’s model [25]. Blue and yellow balls show Si and Au atoms, respectively. (c) 30 × 11 nm² STM image ($V_s = 1.31$ V, $I = 0.5$ nA) illustrating occurrence of the mirror domains.

data and has already been introduced by Jałochowski [34] and Patterson [35].

Patterson [35] have found similarities of STM images available in literature and DFT-simulated STM images based on the 6 × 6 atomic structure proposed by Grozea *et al.* [25], but only in the case when all specific Au sites are occupied. In the present study we went further and compared our high-resolution STM images with DFT simulations for various occupancies of A, B, and C positions. As an example, Fig. 3 shows STM images of the two 6 × 6 unit cells with A position occupied [Fig. 3(a)] and A and B positions occupied [Fig. 3(b)] and corresponding simulated STM images [Figs. 3(c) and 3(d)]. One can see that simulated STM images reproduce all observed features for both experimental STM images. Moreover, simulations reproduce variations in the STM appearance of each specific site (A, B, and C) which depend on whether it is occupied or not [Fig. 3(e)]. This result not only confirms the atomic model, but also allows direct determination of the origin of each type of bright or dim features on the 6 × 6 surface. Using this knowledge and statistics obtained from the STM images, we can now determine atomic structure of the most abundant 6 × 6-Au unit cell.

Higashiyama *et al.* [33] analyzed STM images of the 6 × 6-Au surface prepared with different Au deposition doses. They have found that almost independently of the deposited Au coverage occupation probabilities of A, B, and C sites are 0.81, 0.33, and 0.08, respectively. However, this statistics do not allow the direct determination of the most abundant 6 × 6 unit cell. For example, calculation of the probability to find an unit cell with ABC sites occupied, as simple product of separate A, B, and C occupation probabilities, is not strictly correct, since simultaneous occupation of A, B, and C sites within a given unit cell might be dependent events. To resolve this problem, we calculated both separate A, B, and C probabilities and probabilities to find all eight possible

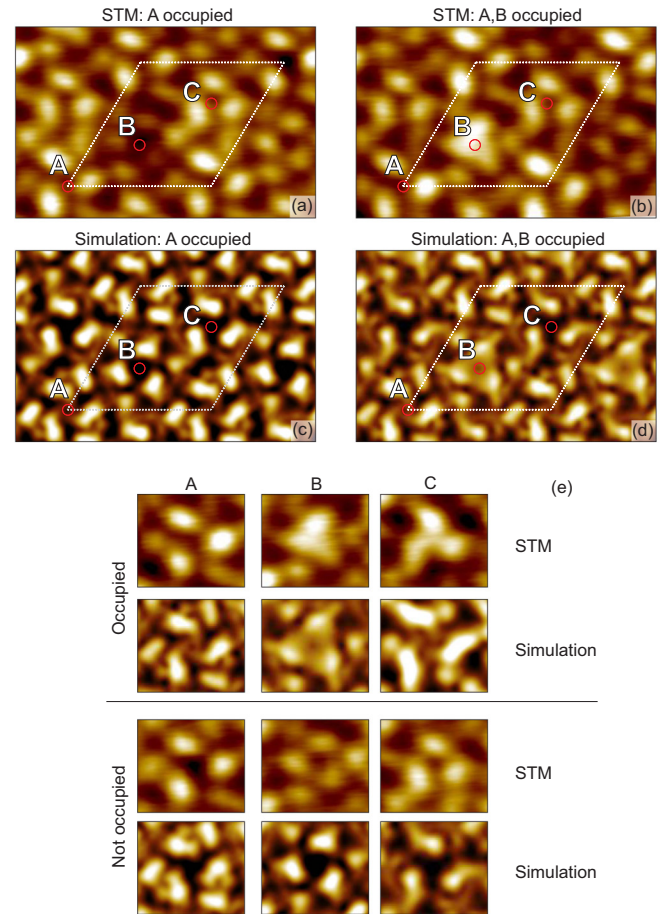


FIG. 3. Comparison of experimental STM images ($V_s = -0.5$ V) with DFT calculated ones for Si(111)6 × 6-Au surface. STM images for 6 × 6 unit cell (a) with A position occupied and (b) A + B positions occupied and (c) and (d) corresponding simulated STM images. (e) Experimental STM images of each specific site (A, B, and C) being occupied and unoccupied in comparison with corresponding simulated STM images.

fillings of 6 × 6-Au unit cell using our STM data set. These results are presented in Table I. Gray cells and white cells in the table contain STM-derived probabilities of A, B, and C sites to be occupied and not occupied, respectively. Column “Product” contains product of A, B, and C probabilities and column “Counted” contains probabilities obtained upon direct counting of the corresponding unit cells in the STM images. As one can see, the present data yield slightly higher separate A, B, and C probabilities than those reported by Higashiyama *et al.* [33]. More important here is that the products of separate probabilities are almost the same as the directly counted probabilities for each type of a cell. Pearson correlation coefficient for columns Product and Counted in Table I is 0.996, which can be classified as a quite strong correlation. This means that Au adsorption onto a given site does not essentially depend on whether the other sites within the unit cell are occupied or not. Such independence of occupancy of A, B, and C sites and their overall random scattering are plausibly related to the small difference in the formation energies for all eight types of 6 × 6 unit cells [(1–9) meV per 1 × 1 unit cell according to the DFT calculations].

TABLE I. Eight possible combinations of 6×6 -Au unit cell specific sites fillings. Gray cells and white cells contain STM-derived probabilities of A, B, and C sites to be occupied and not occupied, respectively. Column “Product” contains product of A, B, and C probabilities and column “Counted” contains probabilities obtained by direct counting of corresponding unit cells in the experimental STM images.

Au atoms	A	B	C	Product	Counted
45	0.92	0.51	0.15	0.069	0.088
44	0.08	0.51	0.15	0.006	0.011
44	0.92	0.49	0.15	0.066	0.047
44	0.92	0.51	0.85	0.399	0.379
43	0.92	0.49	0.85	0.381	0.401
43	0.08	0.51	0.85	0.037	0.035
43	0.08	0.49	0.15	0.006	0.003
42	0.08	0.49	0.85	0.035	0.036

As one can see in the Table I, the two types of 6×6 unit cells dominate on the surface, the A cell with only A position occupied (40% of all unit cells) and the A + B cell with A and B positions simultaneously occupied (38% of all unit cells). In average, the 6×6 unit cell contains 43.58 Au atoms, that corresponds to the Au coverage of 1.21 ML. Statistics reported by Higashiyama *et al.* [33] gave slightly lower Au coverage of 1.20 ML (43.23 Au atoms) with the A cell being more popular (49% of all unit cells) than the A + B cell (24% of all unit cells). This modest discrepancy might be associated with the difference in the 6×6 -Au surface preparation procedures. In the present case, 10 ML of Au was deposited to obtain a well-ordered 6×6 -Au surface, while Higashiyama *et al.* [33] deposited less amount of Au, 1.5 to 3.0 ML of Au. Nevertheless, it seems safe to state that the real 6×6 -Au surface contains ~ 1.2 ML of Au.

B. Si(111) 6×6 -Au: Electronic band structure

Data of available ARPES works [24,37] on electronic band structure of the 6×6 -Au surface are controversial. While Okuda *et al.* [37] described the 6×6 -Au surface as being metallic with two surface-state bands, Zhang *et al.* [24] described it as semiconducting with a small band gap of 50 meV and having eight surface-state bands. The available DFT calculations [35] showed that the surface is metallic with at least six surface-state bands. It is worth noting that direct comparison of the calculated and experimental band structures was hardly possible. First, the energy and momentum resolution of the reported ARPES data [24,37] was insufficient to resolve the 6×6 periodicity. Second, the calculations were done for the 6×6 unit cell with all three sites A, B, and C being occupied [35], while such configuration covers only 9% of the real 6×6 -Au surface (see Table I).

To find the matching between ARPES data and DFT calculations, we performed ARPES measurements with advanced energy and momentum resolution, 15 meV and 0.01 \AA^{-1} , respectively (Fig. 4), and compared them with the DFT calculation for the most abundant 6×6 unit cells occurring at the 6×6 -Au surface (Fig. 5). According to the refined ARPES data (Fig. 4), the surface appears to be metallic

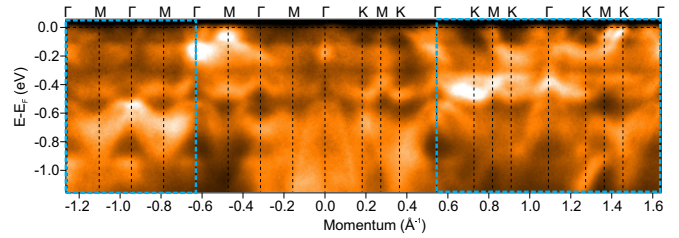


FIG. 4. Experimental ARPES intensity plot measured along the \bar{M} - $\bar{\Gamma}$ - \bar{K} - \bar{M} directions for Si(111) 6×6 -Au surface.

and the observed band dispersions clearly follow the 6×6 periodicity. One can distinguish, at least, five surface-state bands periodically dispersing inside the 6×6 surface Brillouin zone (SBZ), implying that surface has a good crystalline order. Nevertheless, the observed spectral features are mostly smeared and cloudy which can be associated with the surface inhomogeneity in a form of partial occupancy of three Au atomic positions described above. To examine electronic band structure of 6×6 -Au surface in a detail, let us consider results of the DFT calculations.

Figure 5 shows results of DFT band structure calculations for different filling of specific Au atomic positions, including all empty, 42 Au atoms [Fig. 5(a)], A site occupied, 43 Au atoms [Fig. 5(b)], A + B sites occupied, 44 Au atoms [Fig. 5(c)]; A + B + C sites occupied, 45 Au atoms [Fig. 5(d)]. Calculations were made with spin-orbit coupling (SOC) included and it appears that all surface-state bands with contribution from Au atoms are spin split (marked blue in Fig. 5). Spin splitting is considerable and for the metallic band S1 the highest values are around the \bar{M} point: 0.05 \AA^{-1} in momentum and 50 meV in energy. Occurrence of spin splitting here is quite natural, since Au atoms provide strong SOC, which is known to cause a large Rashba-type spin splitting of surface-state bands [16,38–40]. For each of four 6×6 unit cell fillings in Fig. 5, seven pairs of spin-split bands are marked from top to bottom as S0 to S6. Energetic position and shape of each band change with various Au filling. Nevertheless, each band mostly preserves its own features and energetic order of bands does not change. Note, that for the 42 Au case, i.e., all sites empty [Fig. 5(a)], the surface is semiconducting with 30 meV band gap at the Fermi level between the S1 and S2 bands. Addition of an Au atom into the A site (43 Au atoms) leads to incomplete filling of the S1 band and the surface becomes metallic [Fig. 5(b)]. Further Au addition (44 Au atoms, A + B positions occupied) increases electron filling of the S1 band [Fig. 5(c)]. Finally, when all sites are occupied [Fig. 5(d)] the S1 state is completely filled and the S0 band crosses the Fermi level. Overall Au addition to the parent 42-Au-atom structure can be roughly visualized as electron filling of the S1 and S2 bands. ARPES data [Fig. 5(e)] resemble mostly the calculated features of the 43-Au-atom and 44-Au-atom structures, where the S1 band crosses the Fermi level. Bearing in mind that in average there are 43.58 Au atoms per 6×6 unit cell and 78% of the surface is composed of 43-Au-atom and 44-Au-atom configurations, i.e., A and A + B structures, one can conclude that the ARPES results are in a general agreement with the STM statistics.

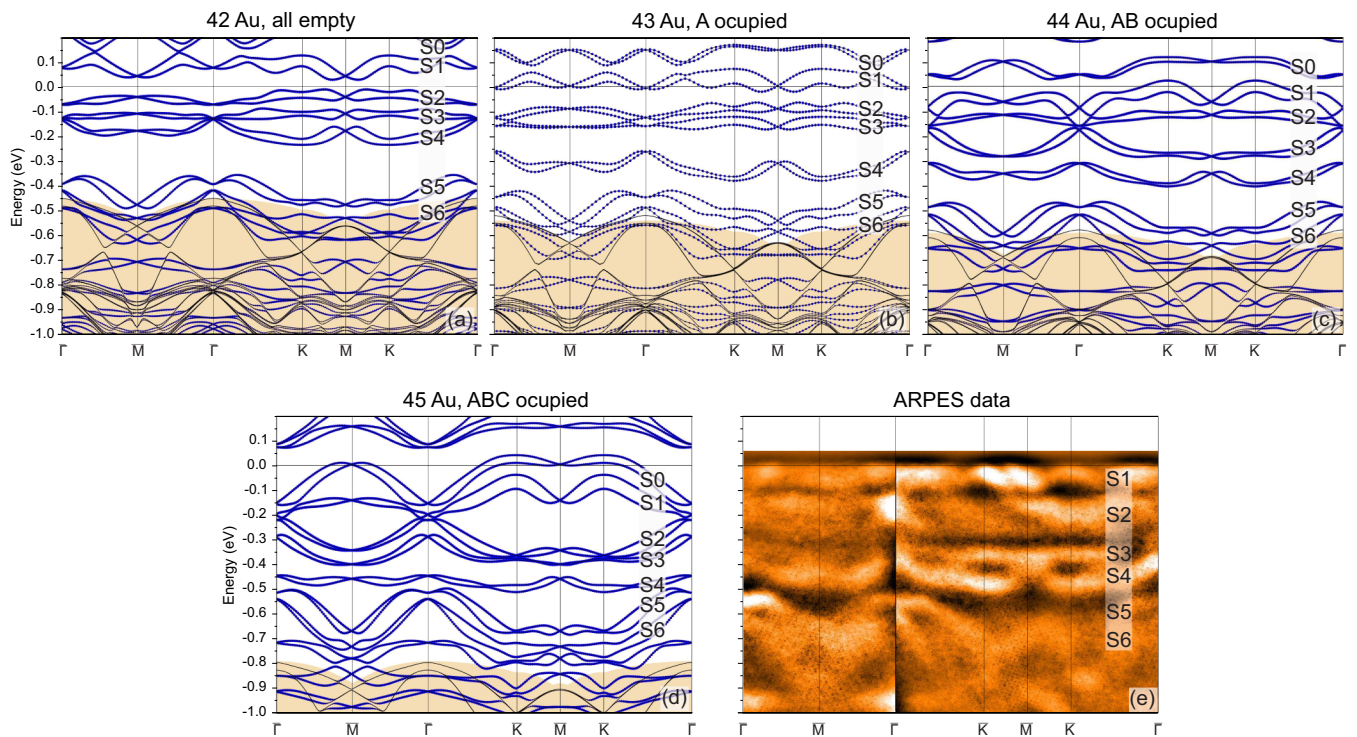


FIG. 5. DFT calculated band structure and ARPES data for 6×6 -Au surface. DFT calculations with different occupation of specific Au atomic positions: (a) all empty, 42 Au atoms per 6×6 -Au unit cell; (b) A site occupied, 43 Au atoms; (c) A + B sites occupied, 44 Au atoms; (d) A + B + C sites occupied, 45 Au atoms. (e) Symmetrized and Gauss filtered ARPES intensity plot of the outlined regions in Fig. 4.

C. Au/Si(111): Domain walls and phase diagram

As mentioned above, the 6×6 -Au atomic model can be visualized as an ordered stacking of the $\sqrt{3} \times \sqrt{3}$ CHCT “nanodomains.” Grozea *et al.* [25] noticed that such stacking produces rectangular pattern with $2 \times \sqrt{3}$ unit cell [outlined by red rectangle in Fig. 6(a)]. They associated these $2 \times \sqrt{3}$ rectangles with the DWs observed at $\alpha - \sqrt{3} \times \sqrt{3}$ -Au and $\beta - \sqrt{3} \times \sqrt{3}$ -Au surfaces. The DW model built in a such way is shown separately in between the $\sqrt{3} \times \sqrt{3}$ CHCT domains in Fig. 6(b) and will be denoted further as a “bridge model,” since four Au trimers in it are simply connected by a “bridge” of two additional Au atoms. This model contains 5 Au atoms per $2 \times \sqrt{3}$ unit cell or 1.25 ML of Au. In the 6×6 -Au surface, the rectangular $2 \times \sqrt{3}$ units surround each nanodomain with Au specific sites inside forming triangular closed DWs. As an example, in Fig. 6(a) DWs formed around the B specific Au site are outlined by blue triangles. Such ordering of the DWs was observed upon heating and slow cooling of the $\beta - \sqrt{3} \times \sqrt{3}$ -Au surface [22–24] and was described in terms of the glass-to-crystal transition [24]. Nevertheless, after the Grozea’s paper [25], no one considered the bridge model of DWs [Fig. 6(b)]. Even in the most recent DFT study [35], another model proposed earlier by Falta *et al.* [26] was treated, where DW is formed by 180° -rotated Au trimers centered in the H_3 sites, instead of the T_4 sites of regular Au trimers. This DW model surrounded by $\sqrt{3} \times \sqrt{3}$ domains was built in an $8 \times \sqrt{3}$ cell to perform DFT calculations. Prior to relaxation, DW contained 1.5 ML of Au compared with 1.0 ML of Au for the regular $\sqrt{3} \times \sqrt{3}$ domains. After relaxation, one Au atom was repulsed from DW reducing the local Au

coverage and causing strong displacement in Au and Si atomic positions in surrounding $\sqrt{3} \times \sqrt{3}$ unit cells [Fig. 6(c)]. In contrast, in the bridge model [Fig. 6(b)] there are no significant displacements for Au and Si atoms in $\sqrt{3} \times \sqrt{3}$ unit cells, implying a lower surface stress. Moreover, present DFT calculations show that the bridge model has formation energy 48 meV per 1×1 unit cell lower than the Falta’s model [26].

Figure 7 presents comparison of the experimental and DFT simulated STM images of a domain wall. It is clearly seen that the bridge model provides the best coincidence. This model reproduces the experimental STM images both in a relative contrast of DW and $\sqrt{3} \times \sqrt{3}$ domain, as well as in a shape of DW itself. Additional proof for the relation between the bridge model and the 6×6 -Au model can be found in the STM image of a larger area of $\alpha - \sqrt{3} \times \sqrt{3}$ -Au surface where small triangular DW closed loops are observed (outlined by blue triangles) [Fig. 7(d)]. These triangles are the smallest possible DW closed loops and essentially are the same blue triangles outlined in the 6×6 -Au atomic model in Fig. 6(a) or, in other words, are the building blocks of the 6×6 -Au surface. Their STM appearance is quite similar to the B-type feature at the 6×6 -Au surface (Fig. 2). Moreover, exactly as at the 6×6 -Au surface there are two mirror types of such triangular loops and they can be dim (occupied) or bright (not occupied), i.e., with or without Au atom inside the loop, as shown in Fig. 7(d).

Present results strongly support the bridge DW model and now, using this model, one can almost fully describe atomic arrangement of the $\alpha - \sqrt{3} \times \sqrt{3}$ -Au and $\beta - \sqrt{3} \times \sqrt{3}$ -Au surfaces built of CHCT $\sqrt{3} \times \sqrt{3}$ domains and domain walls.

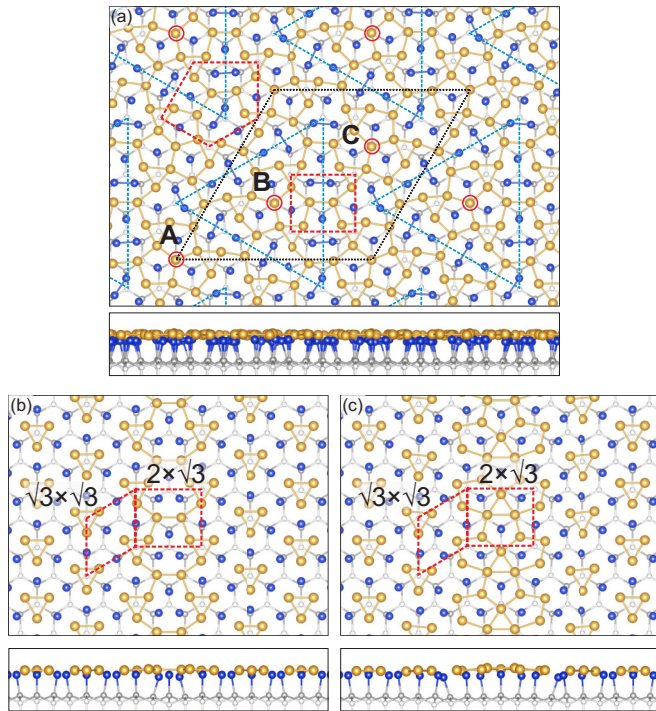


FIG. 6. (a) Atomic structure of 6×6 -Au surface with outlined $2 \times \sqrt{3}$ unit cell of the domain wall. (b) DFT relaxed bridge model of domain wall (extracted from the 6×6 -Au surface model) and the model of domain wall proposed by Falta *et al.* [26]. Blue and yellow balls are Si and Au atoms, respectively, gray and white balls are Si atoms in underlying Si bilayer residing in T_1 and T_4 positions, respectively. Location of A, B, and C specific sites are indicated. Rectangular $2 \times \sqrt{3}$ unit cell of the corner element, and hexagonal $\sqrt{3} \times \sqrt{3}$ unit cell are outlined by red dashed lines. The characteristic triangular building block of the 6×6 structure is outlined by a dashed blue line.

The only lacking element is located at junctions of domain walls with different orientations. Such junctions highlighted at Fig. 7(d) by red pentagons and every junction leads to 240° rotation of DW. Smallest DW loops [blue triangles at Fig. 7(d)] contain three $2 \times \sqrt{3}$ DW elements and three junctions at corners of the loop. Thereby junctions further will be denoted as corner elements. Corner elements are also present at 6×6 -Au surface [red pentagon at Fig. 6(a)]. Similarly to the $2 \times \sqrt{3}$ DW element, one can extract atomic model of the corner element from the 6×6 -Au surface structure. Resulting pentagonal atomic model contains 7.5 Au atoms or 1.15 ML of Au. Now atomic structure of the $\alpha - \sqrt{3} \times \sqrt{3}$ -Au surface is completely resolved and using STM data we can determine its Au coverage. Careful STM area evaluations reveal that the $\sqrt{3} \times \sqrt{3}$ CHCT domains (having Au coverage of 1.0 ML), $2 \times \sqrt{3}$ DWs (having Au coverage of 1.25 ML), and corner elements (having Au coverage of 1.15 ML) occupy 80%, 10%, and 10% of the surface area, respectively. Thus, Au coverage of the $\alpha - \sqrt{3} \times \sqrt{3}$ -Au surface is estimated as 1.04 ML. Note that the evaluations were conducted on the $\alpha - \sqrt{3} \times \sqrt{3}$ -Au surface with Au deficit (in a form of patches of the 5×2 -Au reconstruction with 0.7 ML of Au coverage [20]), hence with the lowest possible density of DWs. Thus, 1.04 ML

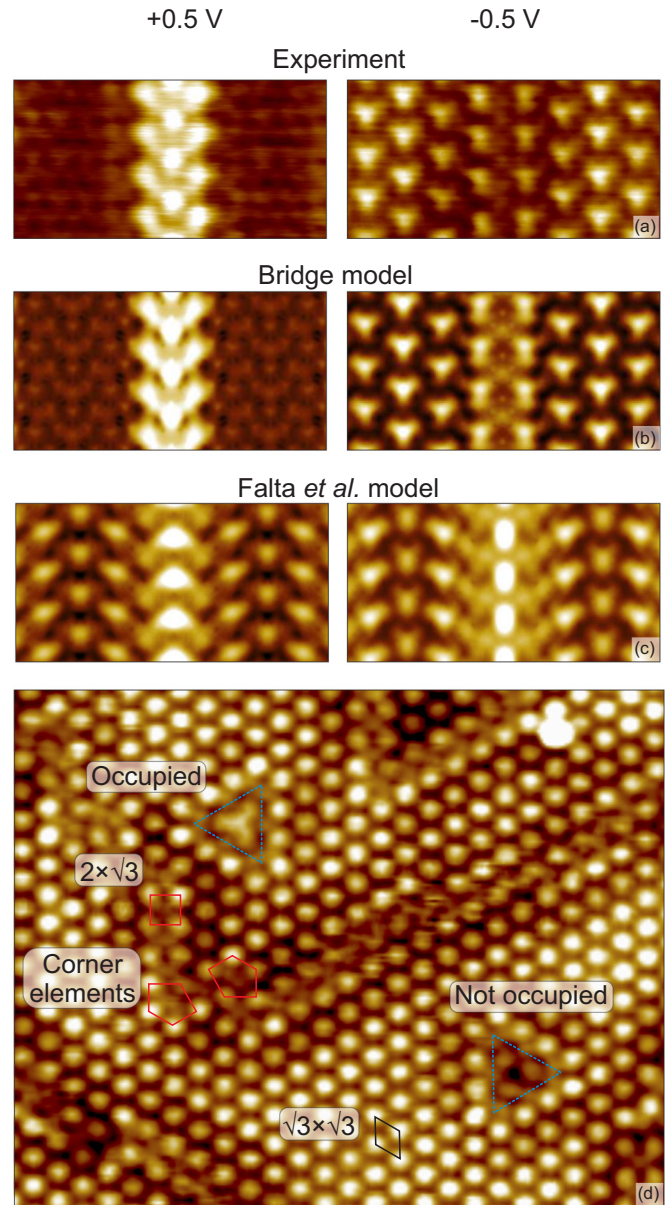


FIG. 7. STM appearance of DWs in the $\alpha - \sqrt{3} \times \sqrt{3}$ phase. Comparison of the experimental STM images (a) measured at different bias voltages (+0.5 and -0.5 V) with DFT simulations (b) and (c) based on bridge [Fig. 6(b)] and Falta's [26] [Fig. 6(c)] atomic models, respectively. (d) STM image ($V_s = -0.96$ V, $I = 0.5$ nA) of $\alpha - \sqrt{3} \times \sqrt{3}$ -Au surface with low density of DWs. The characteristic structural elements (see legend to Fig. 6) are outlined.

is believed to correspond to the minimal Au coverage in the $\alpha - \sqrt{3} \times \sqrt{3}$ -Au surface. Upon increase of the Au coverage the $\alpha - \sqrt{3} \times \sqrt{3}$ -Au surface continuously transforms to the $\beta - \sqrt{3} \times \sqrt{3}$ -Au surface via increasing density of DWs. Remind that the $\beta - \sqrt{3} \times \sqrt{3}$ -Au surface can be reversibly transformed to the 6×6 -Au by heating to 600°C followed by slow cooling [22–24]. Thus, assuming that Au coverage remains unchanged during transformation (e.g., there is a minimal Au exchange with Au three-dimensional (3D) islands usually presented on the surface [41–43]), one can equate Au coverages of $\beta - \sqrt{3} \times \sqrt{3}$ -Au and 6×6 -Au surfaces.

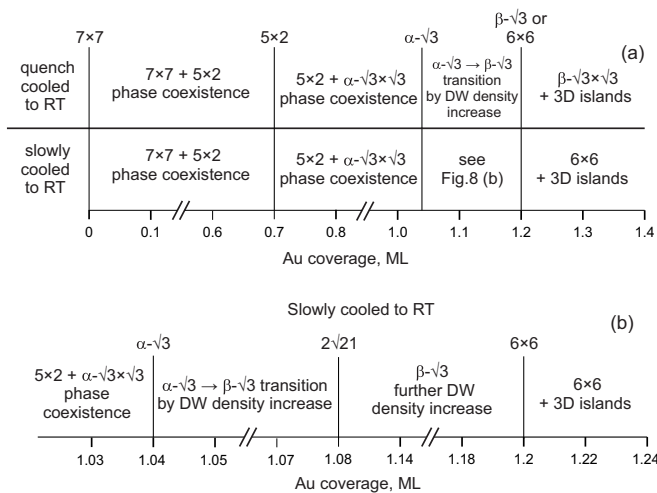


FIG. 8. Schematic of Au/Si(111) formation phase diagram. (a) Different sample preparation procedures after Au deposition and annealing at 600 °C: (top row) quenching (rapid cooling) to RT, (bottom row) slow cooling to RT. (b) Detailed presentation of the region in (a) between 1.04 and 1.2 ML of Au in case of slow cooling to RT.

Therefore, Au coverage of 1.2 ML can be considered as the maximal coverage of the $\beta - \sqrt{3} \times \sqrt{3}$ -Au surface, since its parent ordered structure, 6×6 -Au, has the highest possible density of DWs due to a close packing of the smallest possible DW loops.

With these results, we can now update the long disputed formation phase diagram of Au/Si(111) system [22,43–48]. In the most recent works [43,48], the phase diagrams were built relying on the coverage of the $\alpha - \sqrt{3} \times \sqrt{3}$ -Au as 1.00 ML of Au and as a result the coverage of the 5×2 -Au was underestimated. Figure 8(a) summarizes our findings in a form of simplified diagrams for the two different sample preparation procedures after Au deposition and annealing at 600 °C: (top row) surface is rapidly quenched to RT and (bottom row) slowly cooled to RT. It has recently been shown [20] and then confirmed [43,49–52] that the 5×2 -Au contains 0.7 ML of Au. As discussed above, we found that $\alpha - \sqrt{3} \times \sqrt{3}$ -Au and $\beta - \sqrt{3} \times \sqrt{3}$ -Au surfaces contain 1.04 ML of Au and 1.2 ML of Au, respectively. These data are presented in the top row in Fig. 8(a), where transition from the 5×2 -Au to the $\alpha - \sqrt{3} \times \sqrt{3}$ -Au proceeds through phase coexistence and transition from the $\alpha - \sqrt{3} \times \sqrt{3}$ -Au to the $\beta - \sqrt{3} \times \sqrt{3}$ -Au through increase of the DW density. At 600 °C the Au/Si(111) system is characterized by Stransky-Krastanov growth mode and at Au coverages beyond 1.2 ML deposited Au atoms agglomerate into the 3D islands [41–43]. A more complicated phase diagram is required to summarize the results for the slowly cooled samples [bottom row in Fig. 8(a) and addendum in Fig. 8(b)]. Up to 1.04 ML of Au, everything is the same as for the quenched samples (that was checked in our STM experiments). Results for the slow cooling with Au coverages higher than 1.04 ML are shown in Fig. 8(b).

The $\alpha - \sqrt{3} \times \sqrt{3}$ -Au phase formed at 1.04 ML gradually converts to the $\beta - \sqrt{3} \times \sqrt{3}$ -Au with increasing Au coverage and the DW density. The difference from the case of

the quenched samples resides in the developing of the phase with $2\sqrt{21} \times 2\sqrt{21}$ periodicity (to be discussed later) in the narrow coverage range at about 1.08 ML of Au. When Au coverage exceeds 1.08 ML, the surface transforms back to the $\beta - \sqrt{3} \times \sqrt{3}$ -Au. Finally, at 1.2 ML of Au the 6×6 -Au phase forms and at higher coverages excess Au atoms agglomerate into 3D islands [41–43]. Worth noting that already after formation of the $\alpha - \sqrt{3} \times \sqrt{3}$ -Au surface (i.e., after 1.04 ML of Au) a certain portion of deposited Au can form 3D islands as was shown by low energy electron microscopy [42,43] and x-ray photoelectron spectroscopy [41]. The presented phase diagram (Fig. 8) does not take this into account and in the experiments on the formation of the above described Au-induced reconstructions (with coverage above 1.04 ML of Au) additional Au deposition might be required.

D. Si(111) $2\sqrt{21} \times 2\sqrt{21}$ -Au surface

The $2\sqrt{21} \times 2\sqrt{21}$ -Au surface reconstruction was observed by various research groups after the slow cooling from 600 °C in the coverage range between occurrence of the $\alpha - \sqrt{3} \times \sqrt{3}$ -Au and 6×6 -Au surfaces [4,5,23,24,53] (i.e., between 1.04 and 1.2 ML of Au). This transition, as in the case of 6×6 -Au, was described in terms of the DW ordering [5,23,24], but with the lower Au coverage and, thus, with the lower density of DWs. The only atomic model available in the literature for the $2\sqrt{21} \times 2\sqrt{21}$ -Au surface was proposed by Seifert *et al.* [53] relying on its STM appearance and is built by the ordered stacking of the CHCT $\sqrt{3} \times \sqrt{3}$ domains and inverted Au trimers centered in the H_3 sites. This model is tentative and was not subjected to DFT calculations.

We propose a new model for the $2\sqrt{21} \times 2\sqrt{21}$ -Au surface which is shown in Fig. 9 together with the corresponding experimental and simulated STM images. Construction of the model was based on the thorough examination of the features seen in the high-resolution STM images of the surface and assumption that the structure should incorporate certain elementary blocks characteristic for the $\sqrt{3} \times \sqrt{3}$ CHCT domains, 6×6 -Au surface, and DWs. Thus, the $\sqrt{3} \times \sqrt{3}$ CHCT domains outlined by hexagons in the model [Fig. 9(c)] and simulated STM image [Fig. 9(b)] were placed in the corners of the $2\sqrt{21} \times 2\sqrt{21}$ unit cell. Note that the unit cell contains two inequivalent triangular half-unit cells (HUCs). The inner area of the right HUC outlined by the triangle has STM appearance [Fig. 9(a)] very similar to that of B-type feature of 6×6 -Au surface in Fig. 3(b) recorded with the same STM bias. Such triangular building block of the 6×6 -Au surface was placed in the center of the right HUC. The rest area of the atomic model was constructed bearing in mind that at -0.5 V STM bias Au atoms look bright and areas with Si atoms look dim (as noticed for the $\alpha - \sqrt{3} \times \sqrt{3}$ -Au and 6×6 -Au surfaces), thus by simple matching of STM bright features with Au atoms. Special efforts were undertaken to reach the situation when the structural elements (outlined by squares and circular arcs in Fig. 9) which look symmetric in experimental STM image would be reproduced by symmetric arrangement of Au atoms in the model. Though upon relaxation of the model structure some of Si and Au atoms become slightly shifted from symmetric positions, the simulated STM image [Fig. 9(b)] fairly well reproduces all

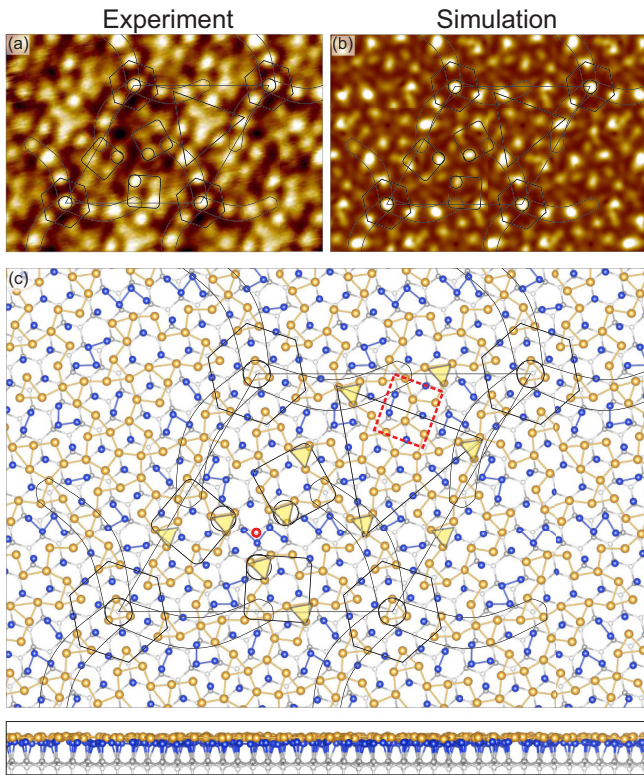


FIG. 9. New structural model of the $2\sqrt{21} \times 2\sqrt{21}$ -Au surface. Comparison of (a) experimental ($V_s = -0.5$ V, $I = 30$ pA) and (b) simulated ($V_s = -0.5$ V) STM images. (c) Atomic model with outlined building blocks. Blue and yellow balls in (c) show Si and Au atoms, respectively, gray and white balls show Si atoms in the underlying Si(111) bilayer residing in the T_1 and T_4 positions, respectively.

the characteristic features of the experimental STM image [Fig. 9(a)]. The model contains 91 Au atoms or 1.08 ML of Au which is only 0.04 ML higher than the coverage of the $\alpha - \sqrt{3} \times \sqrt{3}$ -Au surface (1.04 ML).

The present model differs considerably from the model proposed earlier by Seifert *et al.* [53]. Having only one Au atom more (91 compared with 90 [53]), the present model has a more uniform distribution of Au atoms with smaller CHCT $\sqrt{3} \times \sqrt{3}$ domains and less Au dense areas with the H_3 -centered Au trimers. Note that Au trimers centered in the

H_3 positions [highlighted by yellow triangles in Fig. 9(c)] are distinctive feature of the $2\sqrt{21} \times 2\sqrt{21}$ -Au surface, since at the $\sqrt{3} \times \sqrt{3}$ -Au and 6×6 -Au surfaces only the T_4 -centered Au trimers are present. Moreover, at the $2\sqrt{21} \times 2\sqrt{21}$ -Au surface DW elements [highlighted by red rectangle in Fig. 9(c)] are incomplete and present only at the border of triangular 6×6 -like elements. Thus, formation of the $2\sqrt{21} \times 2\sqrt{21}$ -Au surface apparently cannot be described just by a simple ordering of DWs.

IV. CONCLUSIONS

In conclusion, we demonstrated that the atomic model of the Si(111) 6×6 -Au proposed by Grozea *et al.* [25] is valid as it reproduces obtained STM and ARPES data. Moreover, STM simulation based on this model enabled statistical analysis of the STM images, which yields an averaged 6×6 unit cell with 43.58 Au atoms, i.e., 1.21 ML of Au. Band structure calculated for the most abundant 6×6 unit cells with 43 and 44 Au atoms reasonably reproduces ARPES data, qualifying the 6×6 -Au surface as metallic. We also showed that the atomic model of the domain walls extracted from the 6×6 -Au model provides the best coincidence of the STM data with DFT simulation in comparison with the model proposed by Falta *et al.* [26]. The present model of domain walls contains 5 Au atoms per $2 \times \sqrt{3}$ unit cell or 1.25 ML of Au. For the $\alpha - \sqrt{3}$ and $\beta - \sqrt{3}$ surfaces, these findings allow overall description of their atomic structure and, hence, accurate determination of Au coverage. Basing on the atomic models of the $\alpha - \sqrt{3}$ and 6×6 -Au surface, a new model for the Si(111) $2\sqrt{21} \times 2\sqrt{21}$ -Au surface structure was proposed. It incorporates 91 Au atoms per $2\sqrt{21} \times 2\sqrt{21}$ unit cell or 1.08 ML of Au. Finally, these findings were summarized in the detailed formation phase diagram of Au/Si(111) system.

ACKNOWLEDGMENTS

The work was supported by the Russian Science Foundation under Grant No. 19-12-00101. The part of the work devoted to the ARPES measurements was supported by the Council on grants of the President of the Russian Federation Grant No. MK-343.2019.2. The calculations were conducted using the equipment of Shared Resource Center “Far Eastern Computing Resource” IACP FEB RAS [54].

[1] J. Lander, *Surf. Sci.* **1**, 125 (1964).
 [2] H. E. Bishop and J. C. Rivière, *J. Phys. D: Appl. Phys.* **2**, 1635 (1969).
 [3] T. Okuda, H. Daimon, H. Shigeoka, S. Suga, T. Kinoshita, and A. Kakizaki, *J. Electron Spectrosc. Relat. Phenom.* **80**, 229 (1996).
 [4] E. A. Khramtsova and A. Ichimiya, *Jpn. J. Appl. Phys.* **36**, L926 (1997).
 [5] H. Sakai, E. A. Khramtsova, and A. Ichimiya, *Jpn. J. Appl. Phys.* **37**, L755 (1998).
 [6] I. Collins, J. Moran, P. Andrews, R. Cosso, J. O’Mahony, J. McGilp, and G. Margaritondo, *Surf. Sci.* **325**, 45 (1995).

[7] R. Losio, K. N. Altmann, and F. J. Himpsel, *Phys. Rev. Lett.* **85**, 808 (2000).
 [8] J. L. McChesney, J. N. Crain, V. Pérez-Dieste, F. Zheng, M. C. Gallagher, M. Bissen, C. Gundelach, and F. J. Himpsel, *Phys. Rev. B* **70**, 195430 (2004).
 [9] W. H. Choi, P. G. Kang, K. D. Ryang, and H. W. Yeom, *Phys. Rev. Lett.* **100**, 126801 (2008).
 [10] F. Hötzel, K. Seino, C. Huck, O. Skibbe, F. Bechstedt, and A. Pucci, *Nano Lett.* **15**, 4155 (2015).
 [11] H. S. Yoon, S. J. Park, J. E. Lee, C. N. Whang, and I.-W. Lyo, *Phys. Rev. Lett.* **92**, 096801 (2004).
 [12] E. H. Do, S. G. Kwon, M. H. Kang, and H. W. Yeom, *Sci. Rep.* **8**, 15537 (2018).

- [13] P.-G. Kang, H. Jeong, and H. W. Yeom, *Phys. Rev. Lett.* **100**, 146103 (2008).
- [14] I. Barke, S. Polei, V. v. Oeynhausen, and K.-H. Meiwes-Broer, *Phys. Rev. Lett.* **109**, 066801 (2012).
- [15] F. Hötzel, K. Seino, S. Chandola, E. Speiser, N. Esser, F. Bechstedt, and A. Pucci, *J. Phys. Chem. Lett.* **6**, 3615 (2015).
- [16] L. V. Bondarenko, D. V. Gruznev, A. A. Yakovlev, A. Y. Tupchaya, D. Usachov, O. Vilkov, A. Fedorov, D. V. Vyalikh, S. V. Eremeev, E. V. Chulkov, A. V. Zotov, and A. A. Saranin, *Sci. Rep.* **3**, 1826 (2013).
- [17] F.-C. Chuang, C.-H. Hsu, H.-L. Chou, C. P. Crisostomo, Z.-Q. Huang, S.-Y. Wu, C.-C. Kuo, W.-C. V. Yeh, H. Lin, and A. Bansil, *Phys. Rev. B* **93**, 035429 (2016).
- [18] B. Huang, K.-H. Jin, H. L. Zhuang, L. Zhang, and F. Liu, *Phys. Rev. B* **93**, 115117 (2016).
- [19] Z. Liu, Y. Jin, Y. Yang, Z. F. Wang, and J. Yang, *New J. Phys.* **20**, 023041 (2018).
- [20] S. G. Kwon and M. H. Kang, *Phys. Rev. Lett.* **113**, 086101 (2014).
- [21] Y. Ding, C. Chan, and K. Ho, *Surf. Sci.* **275**, L691 (1992).
- [22] T. Nagao, S. Hasegawa, K. Tsuchie, S. Ino, C. Voges, G. Klos, H. Pfnür, and M. Henzler, *Phys. Rev. B* **57**, 10100 (1998).
- [23] H. M. Zhang, T. Balasubramanian, and R. I. G. Uhrberg, *Phys. Rev. B* **65**, 035314 (2001).
- [24] H. M. Zhang, T. Balasubramanian, and R. I. G. Uhrberg, *Phys. Rev. B* **66**, 165402 (2002).
- [25] D. Grozea, E. Landree, L. Marks, R. Feidenhans'l, M. Nielsen, and R. Johnson, *Surf. Sci.* **418**, 32 (1998).
- [26] J. Falta, A. Hille, D. Novikov, G. Materlik, L. Seehofer, G. Falkenberg, and R. Johnson, *Surf. Sci.* **330**, L673 (1995).
- [27] G. Kresse and J. Hafner, *Phys. Rev. B* **49**, 14251 (1994).
- [28] G. Kresse and J. Furthmüller, *Comput. Mater. Sci.* **6**, 15 (1996).
- [29] P. E. Blöchl, *Phys. Rev. B* **50**, 17953 (1994).
- [30] G. Kresse and D. Joubert, *Phys. Rev. B* **59**, 1758 (1999).
- [31] L. G. Ferreira, M. Marques, and L. K. Teles, *Phys. Rev. B* **78**, 125116 (2008).
- [32] L. G. Ferreira, M. Marques, and L. K. Teles, *AIP Adv.* **1**, 032119 (2011).
- [33] K. Higashiyama, A. Egami, S. Hosoi, and K. Suzuki, *Jpn. J. Appl. Phys.* **40**, 6985 (2001).
- [34] M. Jałochowski, *Prog. Surf. Sci.* **74**, 97 (2003).
- [35] C. H. Patterson, *J. Phys.: Condens. Matter* **27**, 475001 (2015).
- [36] R. Daudin, T. Nogaret, A. Vaysset, T. U. Schüllli, A. Pasturel, and G. Renaud, *Phys. Rev. B* **91**, 165426 (2015).
- [37] T. Okuda, H. Daimon, S. Suga, Y. Tezuka, and S. Ino, *Appl. Surf. Sci.* **121-122**, 89 (1997).
- [38] S. LaShell, B. A. McDougall, and E. Jensen, *Phys. Rev. Lett.* **77**, 3419 (1996).
- [39] M. Hoesch, M. Muntwiler, V. N. Petrov, M. Hengsberger, L. Patthey, M. Shi, M. Falub, T. Greber, and J. Osterwalder, *Phys. Rev. B* **69**, 241401(R) (2004).
- [40] P. Höpfner, J. Schäfer, A. Fleszar, S. Meyer, C. Blumenstein, T. Schramm, M. Heßmann, X. Cui, L. Patthey, W. Hanke, and R. Claessen, *Phys. Rev. B* **83**, 235435 (2011).
- [41] K. Higashiyama, S. Kono, and T. Sagawa, *Jpn. J. Appl. Phys.* **25**, L117 (1986).
- [42] W. Świech, E. Bauer, and M. Mundschau, *Surf. Sci.* **253**, 283 (1991).
- [43] S. Curiotto, F. Leroy, F. Cheynis, and P. Müller, *Surf. Sci.* **632**, 1 (2015).
- [44] G. L. Lay, *Surf. Sci.* **132**, 169 (1983).
- [45] S. Hasegawa and S. Ino, *Int. J. Mod. Phys. B* **07**, 3817 (1993).
- [46] R. Plass and L. D. Marks, *Surf. Sci.* **380**, 497 (1997).
- [47] D. Grozea, E. Bengu, and L. Marks, *Surf. Sci.* **461**, 23 (2000).
- [48] J. Kautz, M. W. Copel, M. S. Gordon, R. M. Tromp, and S. J. van der Molen, *Phys. Rev. B* **89**, 035416 (2014).
- [49] T. Shirasawa, W. Voegeli, T. Nojima, Y. Iwasawa, Y. Yamaguchi, and T. Takahashi, *Phys. Rev. Lett.* **113**, 165501 (2014).
- [50] S. G. Kwon and M. H. Kang, *Phys. Rev. B* **92**, 195301 (2015).
- [51] C. H. Patterson, S. Banerjee, and J. F. McGilp, *Phys. Rev. B* **94**, 165417 (2016).
- [52] M. Liebhaber, B. Halbig, U. Bass, J. Geurts, S. Neufeld, S. Sanna, W. G. Schmidt, E. Speiser, J. Räthel, S. Chandola, and N. Esser, *Phys. Rev. B* **94**, 235304 (2016).
- [53] C. Seifert, R. Hild, M. H. von Hoegen, R. Zhachuk, and B. Olshanetsky, *Surf. Sci.* **488**, 233 (2001).
- [54] <https://cc.dvo.ru>.